



## Atomic-scale insight into the origin of pyridine inhibition of MoS<sub>2</sub>-based hydrotreating catalysts

Burcin Temel<sup>a</sup>, Anders K. Tuxen<sup>b</sup>, Jakob Kibsgaard<sup>b</sup>, Nan-Yu Topsøe<sup>a</sup>, Berit Hinnemann<sup>a,\*</sup>, Kim G. Knudsen<sup>a</sup>, Henrik Topsøe<sup>a</sup>, Jeppe V. Lauritsen<sup>b,\*</sup>, Flemming Besenbacher<sup>b</sup>

<sup>a</sup>Haldor Topsøe A/S, Nymøllevej 55, DK-2800 Kgs. Lyngby, Denmark

<sup>b</sup>Interdisciplinary Nanoscience Center (iNANO), and Department of Physics and Astronomy, Aarhus University, DK-8000 Aarhus C, Denmark

### ARTICLE INFO

#### Article history:

Received 10 November 2009

Revised 25 January 2010

Accepted 2 February 2010

Available online 21 March 2010

#### Keywords:

Hydrotreating catalysis

Hydrodesulfurization

Inhibition

Pyridine

Pyridinium

Scanning tunneling microscopy (STM)

Infra-red Spectroscopy

Density functional theory

MoS<sub>2</sub>

### ABSTRACT

Basic nitrogen-containing compounds such as pyridine are well known to be inhibitors of the hydrodesulfurization (HDS) reaction for the MoS<sub>2</sub>-based catalysts. From an interplay of scanning tunneling microscopy (STM) experiments and density functional theory (DFT) calculations, atomic-scale insight into pyridine adsorption on MoS<sub>2</sub> is obtained. In agreement with previous IR-spectroscopy and DFT studies, the STM results show that the pyridine molecule itself interacts weakly or not at all with the MoS<sub>2</sub> nanoclusters. However, in the presence of hydrogen at the MoS<sub>2</sub> edges, adsorbed species are revealed by STM also at the edges. The calculated DFT energies and simulated STM images allowed us to conclude that these species are pyridinium ions located at the catalytically active brim sites. Furthermore, the DFT results for the vibrational modes of the adsorbed pyridinium species agree well with those observed in earlier IR experiments on high surface alumina-supported MoS<sub>2</sub> catalyst. The adsorption sites appear to be very similar to the brim sites involved in hydrogenation reactions in HDS. Thus, the combined STM and DFT results provide new atomic-scale insight into the inhibition effect of basic N-compounds in HDS and the first direct observation of the adsorption mode of basic N-compounds on the catalytically active MoS<sub>2</sub> edges. Our results lend further support to previously reported correlations between inhibiting strength and proton affinity for the N-containing compounds.

© 2010 Elsevier Inc. All rights reserved.

### 1. Introduction

The increasingly more stringent legislative demands for removing sulfur and producing cleaner fuels have introduced new hydro-treating challenges for the refining industries [1]. Specifically, in order to meet present and future specifications [2] for ultra-low sulfur fuels [1,3–11] with low levels of sulfur and nitrogen compounds, improved activity and selectivity of the HDS catalysts are required. Consequently, increased research efforts are devoted to obtain an improved atomic-scale understanding of the structure, reactivity and inhibition mechanism of MoS<sub>2</sub>-based hydrotreating catalysts.

Much of the earlier research has suggested that hydrodesulfurization (HDS) reactions of sulfur-containing compounds occur at characteristic brim sites at the edges of MoS<sub>2</sub> nanoclusters and that HDS can take place following two different pathways: the hydrogenation (HYD) pathway, in which several hydrogenation steps pre-

\* Corresponding authors. Fax: +45 45279999 (B. Hinnemann), +45 86120740 (J.V. Lauritsen).

E-mail addresses: [behi@topsoe.dk](mailto:behi@topsoe.dk) (B. Hinnemann), [jvang@inano.au.dk](mailto:jvang@inano.au.dk), [jvang@phys.au.dk](mailto:jvang@phys.au.dk) (J.V. Lauritsen).

cede sulfur extrusion, and the direct desulfurization (DDS) pathway [1,12,13]. For simple S-compounds, the DDS pathway has been shown to be the most important route [1,4,12]. However, this pathway is often suppressed for sterically hindered alkyl-substituted compounds such as 4,6-dimethyldibenzothiophene (DMDBT), and the HYD pathway may become the dominating route since it is less sensitive to steric effects [4]. Thus, as crude oils become heavier and contain an increasing amount of refractory compounds, the HYD activity is becoming increasingly more important [4,5,7,14]. However, an efficient use of the HYD pathway is complicated by the fact that heterocyclic nitrogen-containing compounds such as pyridine or quinoline, which are typically present in heavy crude oils, severely inhibit the HYD route [1,7,10,15–25]. Ideally, one could alleviate this problem by removing these N-compounds by hydrodenitrogenation (HDN) processes before sulfur is removed by HDS [1,3–5,7,10,12,14–16,20–22,24,26–33], but, HDN is often slower than HDS, and it is therefore imperative to understand the origin of the N inhibition in order to minimize its effect.

For non-sterically hindered heterocyclic compounds with nitrogen in a six-membered ring, it has been shown that the equilibrium adsorption constants, which are used as a measure of

inhibition strength, correlate well with proton affinities of the inhibitor molecules [16,26]. It was proposed that this correlation is due to the interaction of nitrogenous molecules with Brønsted acid sites on the edges of the MoS<sub>2</sub> nanoclusters and that those species that tend to get protonated easier adsorb on the catalyst surface more strongly. Subsequent IR studies [34] of pyridine adsorption on alumina-supported MoS<sub>2</sub> catalyst did indeed show the presence of Brønsted acid sites as indicated by the presence of pyridinium ion, which gives rise to a characteristic IR band at 1546 cm<sup>-1</sup>. The fact that the pyridinium ion was not observed at room temperature but first at higher temperatures indicated that the protonation was activated such that high temperature was required to activate the proton transfer from the SH group to pyridine [18,34].

The nature of the active sites for the HYD and DDS pathways has been much debated in the literature. Early studies [1,31,35] have considered multiple vacancy sites or “naked” MoS<sub>2</sub> edge sites, i.e., the Mo-edge in its stoichiometric termination without the presence of the strongly bonded sulfur atoms [36]. Recently, combined STM [37–40] and DFT studies [41–48] have allowed one to revisit many of the earlier proposals for HYD and DDS sites since these methods have provided unique insight into the structures of MoS<sub>2</sub> nanoclusters. Extensive edge reconstructions may take place, and the structures are typically very different from those proposed in the past (as in the “naked” Mo-edges) where it was assumed that the edges have structures with atoms occupying bulk-like lattice positions [44,45,47]. It was furthermore revealed that the shape of MoS<sub>2</sub> nanoclusters depends significantly on the composition of the surrounding gas that is whether they are exposed to sulfiding or reducing gas conditions. Specifically, MoS<sub>2</sub> clusters may have a triangular shape with only the (10 $\bar{1}$ 0) Mo-edge exposed under sulfur-rich conditions, whereas they depict a hexagonal morphology and expose both the Mo-edge and the ( $\bar{1}$ 010) S-edge under HDS conditions. Surprisingly, high resolution images also revealed a characteristic bright brim structures at the edges of MoS<sub>2</sub> nanoclusters (referred as the brim sites) [37,38,40–44,49], which were identified by DFT to be metallic edge states. Subsequent STM and DFT studies showed that these sites may play an important role for both hydrogenation and C–S bond scission.

Based on the improved atomic-scale understanding of the MoS<sub>2</sub> edges, it has recently been possible to provide insight into the details of active sites and reaction pathways for both the HYD and the DDS pathway of thiophene [31,50]. Pyridine inhibition was treated in a DFT study by Logadottir et al. [51]. They found that the pyridine molecule only interacts weakly with the MoS<sub>2</sub> nanoclusters. However, on the Mo-edge, pyridine can be protonated to pyridinium with a very low barrier, and the resulting pyridinium binds much stronger than pyridine. In contrast, on the S-edge, formation and binding of pyridinium was not found to be favorable. These results provided additional evidence for pyridinium formation as the main origin of the inhibition and furthermore pointed out that inhibition is different at the two edges.

Although the previous studies have provided evidence for pyridinium formation on MoS<sub>2</sub>, the exact bonding configuration has never been addressed directly. In the present combined STM and DFT study, we provide the first direct evidence for the presence and location of pyridinium on MoS<sub>2</sub>. In addition, we have carried out a detailed DFT analysis of the vibrational frequencies of different adsorbed species to further elucidate the previous IR results on pyridine adsorption [34]. Finally, the DFT results also allow us to gain more fundamental atomic-scale insight into the interaction of pyridine with MoS<sub>2</sub> nanoclusters and the origin of the inhibiting role of N-containing cyclic compounds. We find that only protonated pyridine species (pyridinium, C<sub>5</sub>H<sub>5</sub>N-H<sup>+</sup>), and not pyridine itself, adsorb strongly and especially block the active hydrogenation sites on the Mo-edge of MoS<sub>2</sub> under all relevant catalytic conditions.

## 2. Methods

### 2.1. Scanning tunneling microscopy experiments

The STM experiments were performed on a HDS model system consisting of MoS<sub>2</sub> nanoclusters synthesized on a chemically inert Au substrate in an ultra-high vacuum (UHV) chamber with a base pressure below  $1 \times 10^{-10}$  mbar. The experimental setup was equipped with standard utilities for surface preparation and characterization, and the home built variable temperature Aarhus STM [52] that has been proven capable of routinely achieving atomic resolution on MoS<sub>2</sub> nanoclusters in a number of recent studies (see e.g. [6,38,39]). In the study, the STM image was recorded at temperatures ranging from 160 K to room temperature.

The sample was a planar model catalyst system consisting of highly dispersed perfectly crystalline single-layer MoS<sub>2</sub> nanoclusters that are found to adopt characteristic triangular equilibrium shapes under the present sulfiding conditions. The crystalline MoS<sub>2</sub> nanoclusters were synthesized by evaporating metallic Mo onto an Au(1 1 1) substrate followed by post-annealing the sample at 673 K in a sulfiding H<sub>2</sub>S atmosphere. In several past studies, this procedure has proven to lead to very uniform and well-characterized ensembles of MoS<sub>2</sub> nanoclusters with a known atomic structure at the edges of the clusters edges. These MoS<sub>2</sub> nanoclusters are ideally model systems suited for addressing the atomic-scale details of the active sites on MoS<sub>2</sub> in HDS. The full details concerning the preparation and characterization of the HDS model system and the atomic details of the MoS<sub>2</sub> nanoclusters have been published previously [40,52]. Pyridine (C<sub>5</sub>H<sub>5</sub>N) (Sigma Aldrich, 99% purity) was purified by several freeze-pump-thaw cycles and dosed into the UHV chamber through a leak-valve and a stainless steel tube directed toward the sample. The substrate temperature during pyridine exposure was throughout the experiments controlled by cooling a separate sample stage with liquid nitrogen, and molecules could be dosed at here sample-temperatures ranging from 200 K up to room temperature. We used the maximum temperature of the sample recorded during pyridine dosage as the experimental adsorption temperature and not the actual temperature of STM imaging that was 20–30 K lower.

The role of sulfur vacancies and S–H groups as Brønsted acid sites for protonation of the adsorption of pyridine on the edges was systematically investigated by exposing the MoS<sub>2</sub> nanocluster to atomic (pre-dissociated) hydrogen, with hydrogen being pre-dissociated on a hot (~2000 K) tungsten filament. Molecular hydrogen generally does not lead to the formation of S–H groups and vacancies at UHV-compatible pressures less than  $1 \times 10^{-6}$  mbar, since the hydrogen adsorption at the fully sulfided Mo-edge was shown to be endothermic in a previous study [39]. The atomic H flux was obtained by a standard procedure involving backfilling of the UHV chamber with hydrogen to a pressure of  $1 \times 10^{-6}$  mbar while a very hot tungsten filament used for dissociating the H<sub>2</sub> gas was kept at a 100 mm distance of the sample.

### 2.2. Density functional theory

The density functional theory (DFT) calculations were carried out using an infinite stripe model of MoS<sub>2</sub>, analogous to the results in Refs. [42,44,53]. The equilibrium ( $\bar{1}$ 010) S-edge and (10 $\bar{1}$ 0) Mo-edge of the stripe are shown in Fig. 1. To enable the correct sulfur dimer pairing at the edges, the slab should contain even number of Mo atoms in the x-direction. The supercell in this study contained four Mo atoms both in the x and in the y-directions, in order to avoid replica interactions and to ensure sufficient decoupling between the Mo- and S-edges. Some of the calculations were also repeated with a  $4 \times 6$  supercell; however, the differences in

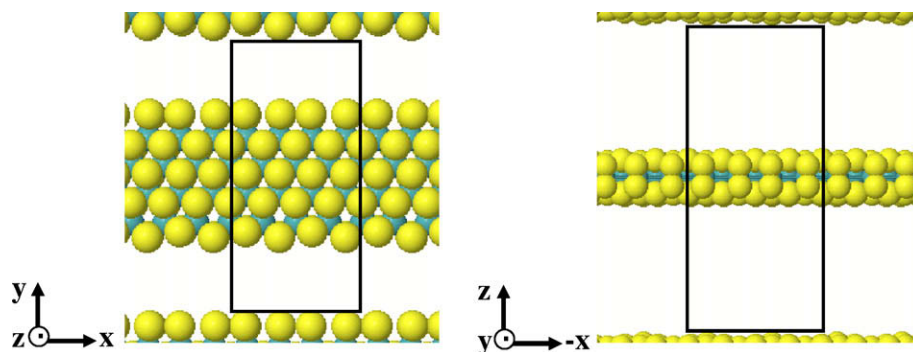


**Fig. 1.** Super cell used in this study. Left: Top view, upper part of the slab is the Mo-edge (with paired S-dimers), and bottom part is the S-edge (with S-dimers). Right: Side view, facing Mo-edge with S-dimers. Color code: sulfur (yellow), molybdenum (green). (For interpretation of the references to color in this figure legend, the reader is referred to the web version of this article.)

results were negligible. The stripes were separated by 14.8 Å in the z-direction (including pyridine) and 9 Å in the y-direction.

The DFT calculations were carried using the DACAPO code [54,55], which utilizes plane-wave basis sets and ultrasoft pseudopotentials. The Brillouin zone was sampled by a Monkhorst–Pack *k*-point set [56] with four *k*-points in the *x*-direction and with one *k*-point in the *y* and *z*-directions. We used a 30 Rydberg plane-wave cutoff and 45 Rydberg density-wave cutoff. Ultrasoft pseudopotentials [57] were used except for sulfur, for which a soft pseudopotential is used as in an earlier study [58]. The ultrasoft sulfur pseudopotential has also been tried in several studies [42–44,53] with similar convergence results to the soft one. We decided to keep the soft sulfur pseudopotential to be able to compare our results to the earlier study [51] in a consistent way. The Fermi temperature was chosen to be  $k_B T = 0.1$  eV, and all the energies were extrapolated to zero electronic temperature. The PW91 exchange correlation functional was used in all the calculations [59], and the convergence criterion for the atomic relaxation was a maximum force of 0.02 eV/Å per atom.

Simulated STM images represented as constant current local density of state images (LDOS) contours were calculated within the simple Tersoff–Hamann formalism [60,61], with the same tunneling conductance parameters that were used in an earlier publication [44], since they were calibrated such that the calculated corrugation on the basal MoS<sub>2</sub> plane matches the experimentally observed ones. Both an s-type tip with a contour value  $\rho(r_0, \varepsilon_F) = 8.3 \times 10^{-6}$  (eV Å<sup>3</sup>)<sup>-1</sup> and a p-type tip with the same contour value were tried in the DFT-based STM simulations, but only the s-type tip results are reported here since the results for the p-type tip did not change the STM images noticeably. The color scale of the STM images is black → red → yellow and corresponds to a corrugation of 3.4 Å. All STM simulations were performed initially on the 4 × 4 unit cell, which allowed us to calculate the STM contours for a large number of structures. All the relevant structures were recalculated using a 4 × 6 unit cell, where the two edges are better separated. Although no significant changes were observed between results for the two unit cells, the structure of the Mo-edge was more clearly visible with the larger unit cell simulation. The 4 × 6 unit cell was used for all STM simulations in the paper, whereas additional structures using the 4 × 4 unit cell are presented in the [Supplementary material](#). Although the STM experiments were done on Au(1 1 1) support, we did not include the support in our calculations since the edge effects are not changed significantly in the absence of Au(1 1 1) [44,62].

The calculations of the vibrational frequencies for comparison with the IR spectra recorded on the high surface catalyst were performed using numerical derivatives obtained by three-point finite differences with 0.02 Å displacements. To limit the computational

time, only the atoms of the adsorbate, including the hydrogen atom of pyridinium ion, were allowed to vibrate, and this gives us all the modes related to the adsorbate molecule. In many studies, it is common to scale the calculated value made here due to the small difference between them (1588 cm<sup>-1</sup> vs. 1592 cm<sup>-1</sup> for measured and calculated, respectively). All the calculated frequencies between 1400 and 1650 cm<sup>-1</sup> of the adsorbates are presented here, and it is found that they match the experimental values very well (differences less than 14 wavenumbers for characteristic peaks).

The adsorption energies were calculated using the following equation:

$$\Delta E_{\text{ads}} = E_{\text{molecule/MoS}_2\text{structure}} - E_{\text{MoS}_2\text{structure}} - E_{\text{molecule(g)}} \quad (1)$$

where  $E_{\text{molecule/MoS}_2\text{structure}}$  is the energy of the system with the molecule bound to the surface,  $E_{\text{MoS}_2\text{structure}}$  is the energy of the relevant starting surface structure and  $E_{\text{molecule(g)}}$  is the energy of the molecule in vacuum. The figures were made using Visual Molecular Dynamics (VMD) [63] and JMol [64].

### 3. Results and discussion

#### 3.1. STM and DFT results on pyridine adsorption on MoS<sub>2</sub>

By means of STM technique, we are able to image the structure and adsorption site of single molecules adsorbed on the MoS<sub>2</sub> edges. In the experiments reported here, we selectively probe the pyridine adsorption on fully sulfided and partially S–H covered MoS<sub>2</sub> Mo-edges and thereby address the atomic-scale structures reflecting the interaction between pyridine and the edges of the MoS<sub>2</sub> nanoclusters. Fig. 2a depicts an atomically resolved STM image of triangular single-layer MoS<sub>2</sub> nanoclusters before adsorption of hydrogen and pyridine. The atomic-scale structure of such MoS<sub>2</sub> nanoclusters has been characterized in great detail previously [37,38,40,49], and it is established that the edges terminating the MoS<sub>2</sub> nanoclusters under sulfiding conditions are Mo-edges that are fully saturated with sulfur dimers (S<sub>2</sub>) (see ball model in Fig. 2). The protrusions on the edges are in all atom-resolved STM images found to be out of registry with respect to the S protrusions on the basal plane of the MoS<sub>2</sub> nanoclusters, and furthermore, the row of edge protrusions are revealed to exhibit a distinct double periodicity. These are exactly the two characteristics that according to previous DFT simulations [39,43] unambiguously identify the edge structure (Fig. 2a). The out of registry effect is a purely electronic effect correlated with the fact that STM probes the local density of states (LDOS) at the Fermi level, and for the S-dimers saturating the Mo-edges, it appears that the maximum LDOS is located in between the S-dimers. A third very important



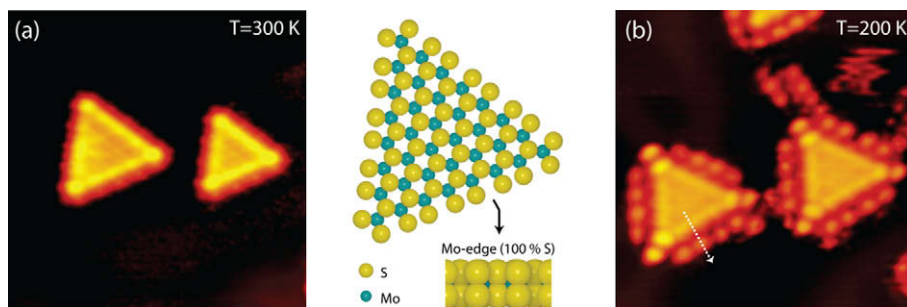


**Fig. 2.** (a) Atom-resolved STM image ( $95 \text{ \AA} \times 95 \text{ \AA}$ ) of single-layered  $\text{MoS}_2$  nanoparticles exposing the fully sulfided Mo-edge. The structure of the triangular  $\text{MoS}_2$  nanoparticles is illustrated in the ball model (top view), and the edge structure is shown as a side view ball model Mo: blue, S: yellow. (b) STM image of two  $\text{MoS}_2$  nanoclusters after exposure to pyridine at 200 K ( $103 \text{ \AA} \times 103 \text{ \AA}$ ). (For interpretation of the references to color in this figure legend, the reader is referred to the web version of this article.)

feature of the  $\text{MoS}_2$  edges is the characteristic bright brim [43] located at the perimeter of the nanoclusters (see Fig. 2a), which is a one-dimensional (1D) metallic edge state at the rim of the  $\text{MoS}_2$  nanoclusters. Previous STM studies and DFT calculations on  $\text{MoS}_2$  nanocluster model have shown that the metallic brim states exhibit unique catalytic properties, since a hydrogenation reaction and subsequent C–S cleavage were observed to proceed at these active brim sites [38]. A recent combined STM and DFT study [39] has indeed demonstrated that the HYD reaction pathway takes place first via adsorption on the brim sites under sulfiding conditions. Furthermore, a DFT study of thiophene HDS under hydrotreating conditions also showed that the HYD pathway can take place on the Mo-edge brim sites without vacancy creation, whereas the DDS pathway may only involve S-vacancies on the edges [50]. To address the fundamental properties of HDS inhibition by pyridine and in particular its role in blocking the HYD reaction pathway, it is therefore very important to clarify the adsorption of pyridine on the brim sites of the  $\text{MoS}_2$  nanoclusters.

### 3.1.1. Adsorption of pyridine on the fully sulfided Mo-edge

To investigate the interaction between pyridine and the fully S-saturated Mo-edges of the  $\text{MoS}_2$  nanoclusters (Fig. 2a), we first dose pyridine both at room temperature (RT) and at 200 K. The STM images at room temperature show no adsorption of pyridine,

neither on the  $\text{MoS}_2(0001)$  basal plane nor at any edge sites. At the lower temperature of 200 K, pyridine molecules are, however, observed to be adsorbed near the edges of  $\text{MoS}_2$  nanoclusters, as seen in Fig. 2b. Individual pyridine molecules are clearly seen at the cluster edges in Fig. 2b, and they appear in the STM images with a slightly lower height relative to the basal plane of the triangular  $\text{MoS}_2$  nanoclusters, and with dimensions ( $\sim 5 \text{ \AA}$  diameter) and shape (circular protrusions) matching approximately the expected symmetry and van der Waals shape of pyridine. These protrusions observed in the STM images are attributed to intact individual pyridine molecules adsorbed on the gold substrate next to the edges of the  $\text{MoS}_2$  nanoclusters. The pyridine molecules adsorbed in these sites next to the  $\text{MoS}_2$  nanoclusters are however adsorbed fairly weakly since after annealing of the sample to  $\sim 300 \text{ K}$ , the adsorbed pyridine molecules were all desorbed. Even at the lowest sample temperature of  $\sim 200 \text{ K}$ , no pyridine molecules were observed on top of the cluster edges at the brim sites of the  $\text{MoS}_2$  nanoclusters, which have previously been shown to act as adsorption sites for thiophene ( $\text{C}_4\text{H}_4\text{S}$ ) under similar conditions [49]. This result thus indicates that the direct interaction of pyridine with fully sulfided  $\text{MoS}_2$  is indeed very weak.

In accordance with the experimental findings, our DFT calculations for pyridine adsorption (Table 1) show that adsorption energies for pyridine on the fully sulfided Mo-edges are in all

**Table 1**

The investigated adsorption sites and energies of pyridine ( $\text{C}_5\text{H}_5\text{N}$ ) on the fully sulfided Mo-edge with S-dimers at 0% or 12.5% S–H coverage. The color code is: sulfur (yellow), molybdenum (green), nitrogen (blue), carbon (gray) and hydrogen (white). (For interpretation of the references to color in this table legend, the reader is referred to the web version of this article.)

Configuration	a	b	c	d
Mo-edge with S-dimers				
Top view				
Side view	H coverage (%) 12.5	H coverage (%) 12.5	H coverage (%) 0	H coverage (%) 0
	$\Delta E_{\text{ads}}$ (eV) –0.20	$\Delta E_{\text{ads}}$ (eV) –0.19	$\Delta E_{\text{ads}}$ (eV) –0.14	$\Delta E_{\text{ads}}$ (eV) –0.20

configurations very small ( $\sim -0.2$  eV). The most favorable configurations (c and d) are associated with an interaction at the brim sites of the fully sulfided Mo-edge. These adsorption energies are slightly exothermic, but the lowest achievable temperature during pyridine dosing in this experiment (200 K) still does not allow a direct observation of these weakly bound pyridine species adsorbed on the brim. In addition, Logadottir et al. [51] have previously shown that pyridine adsorption on the  $\text{MoS}_2(0001)$  basal plane is thermo-neutral under HDS reaction conditions, which is in full accordance with the STM experiments in which no molecules are observed on the basal plane at any time. In the same study, authors have also studied pyridine adsorption on both Mo- and S-edges and found out that the pyridine adsorption is most favorable at the S-edge on a vacancy by 0.28 eV.

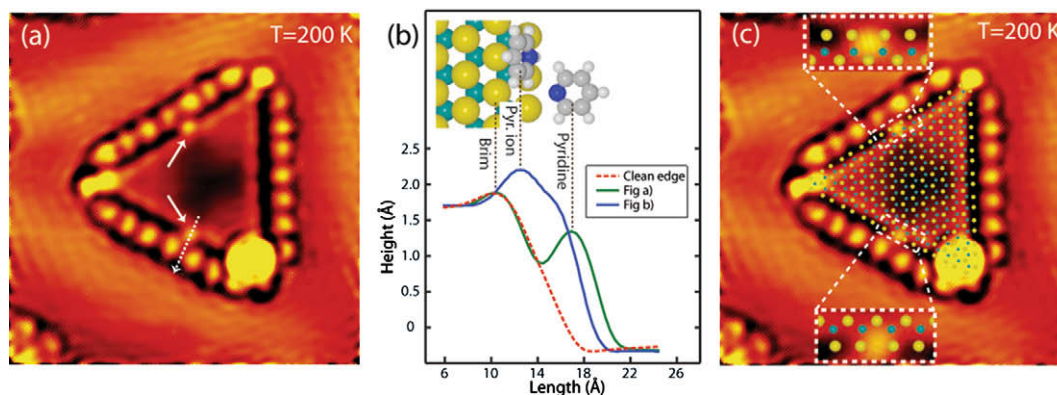
### 3.1.2. Adsorption of pyridine on the fully sulfided Mo-edge with S-H groups

Previous IR studies [34] of adsorption of pyridine on the  $\text{MoS}_2/\text{Al}_2\text{O}_3$  catalyst showed the presence of pyridinium ions, and recent DFT results [51] have proposed that pyridine adsorbed on the brim sites stabilized by H from the SH groups at the Mo-edge. In view of the previous IR-spectroscopy studies [34] and DFT findings related to strong adsorption of pyridinium on the  $\text{MoS}_2$  edges, a second series of STM experiments was performed where hydrogen was dosed to the  $\text{MoS}_2$  nanoclusters. In order to mimic the chemical potential of H at the high partial pressure during HDS reaction conditions, pre-dissociated (atomic) hydrogen was used in the STM experiments. Similar exposures to atomic H have in previous STM studies been found to create a number of isolated sulfur vacancies (0–2 pr. nanocluster) and lead to the formation of S–H groups on the edge region of the  $\text{MoS}_2$  nanoclusters [37–39]. Fig. 3a shows the STM image of a  $\text{MoS}_2$  nanocluster recorded at 200 K after first dosing pyridine at the low temperature and then a subsequent dosing of atomic hydrogen to activate the cluster edges. Again, weakly adsorbed pyridine molecules are identified on the Au substrate next to the  $\text{MoS}_2$  nanoclusters, which we tentatively associate with a physisorbed state of pyridine due to the low temperature. However, in addition, a second type of adsorbed molecule is now also observed as a slightly smaller bright protrusion located on top of the  $\text{MoS}_2$  nanoclusters adjacent to the brim sites (marked with the two solid white arrows in Fig. 3a). These species are more strongly bound to the  $\text{MoS}_2$  nanoclusters, since the associated protrusions can be imaged by STM in the same configuration on the  $\text{MoS}_2$  edges even after heating the sample to temperatures above 400 K. The line scans in Fig. 3b show the detailed sites and corrugation associated with the strongly adsorbed species

relative to line scans obtained on a clean  $\text{MoS}_2$  nanocluster edge (Fig. 2a) and line scans recorded with pyridine physisorbed on the  $\text{MoS}_2$  edges (Fig. 2b). The protrusions associated with the strongly adsorbed species are located on top of the edge state of  $\text{MoS}_2$  nanoclusters and shifted approximately 0.3 nm from the center of the brim state. To further pinpoint the lateral location of the more strongly adsorbed species, we present in Fig. 3c an STM image with the atomic S lattice of the  $\text{MoS}_2$  nanoparticle being superimposed. As seen from the zoom-in STM images inserted in Fig. 3c, it can be determined that the protrusions adjacent to the brim sites are located at a position a slightly shifted inwards from the brim site at the edges of the  $\text{MoS}_2$  nanoclusters, between two edge sulfur atoms. From a detailed analysis of several STM images, we find that the protrusions and thus the strongly adsorbed species always are located at the metallic brim site between two sulfur atoms.

The stronger bonding of the adsorbed species in Fig. 3a and c clearly indicates the presence of a chemisorbed species different from pyridine, which we in view of the previous IR-spectroscopy [34] and DFT findings [51] tentatively attribute to pyridinium ions ( $\text{C}_5\text{H}_5\text{N-H}^+$ ) formed by the protonation of pyridine by  $\text{H}^+$  transfer from an S–H group. To gain further insight into the configurations of the strongly adsorbed species observed in Fig. 3a and b, we performed DFT calculations on adsorbed pyridinium and calculated the corresponding simulated STM images. Since the  $\text{MoS}_2$  nanoclusters are activated by exposure to atomic H, we include in the calculations both the possibility of adsorption of pyridinium on the fully sulfided Mo-edges with a fractional S–H coverage (Table 2) as well as the adsorption of pyridine and pyridinium on the Mo-edge with a sulfur vacancy (Table 3), where the latter can occur by a proton transfer from a nearby surface SH group. Only the results for the most stable configurations are shown in Tables 2 and 3, whereas the remaining investigated configurations are listed in the Supplementary material.

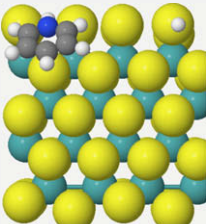
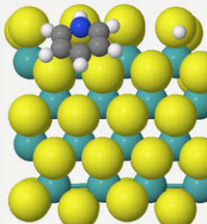
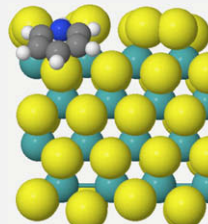
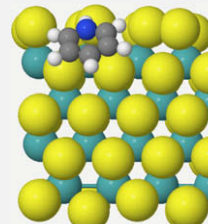
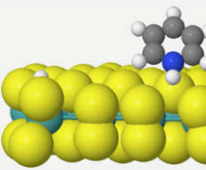
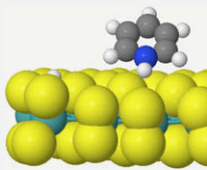
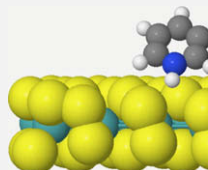
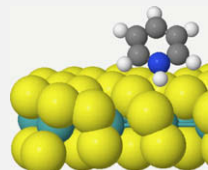
The results for the pyridinium adsorption in Table 2 show that the configurations are all exothermic, indicating that pyridinium ion, formed through a proton transfer to pyridine, is stable at the Mo-edge. The strongest binding occurs when the nitrogen atom of pyridinium ion is located between two sulfur atoms (Table 2, configuration c). As a secondary effect, the presence of surface SH groups is observed to further increase the binding of pyridinium by about 0.5 eV (Table 2, configurations a and b), and the calculations show that adsorption between the two sulfur atoms is indeed favored. Since the SH group is located far away from the adsorbed pyridinium ion, the stabilizing effect of the SH group is due to large rearrangements of the sulfur dimers upon hydrogen adsorption. The DFT results further show that pyridinium is adsorbed much



**Fig. 3.** (a)  $\text{MoS}_2$  nanoparticle after exposure to pyridine and subsequent exposure to atomic hydrogen at 200 K ( $100 \times 100 \text{ \AA}^2$ ). The two solid lines are marking the formed pyridinium ions. (b) Line scans of the dashed lines in (a) in Fig. 2 and (b) in Fig. 3 with a clean Mo-edge as reference. (c) The STM image in (a) with the atomic lattice of a  $\text{MoS}_2$  triangle superimposed. The two close-up images show the detailed location of the protrusions positioned between two edge sulfur atoms.

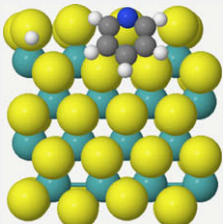
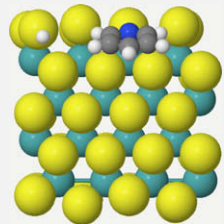
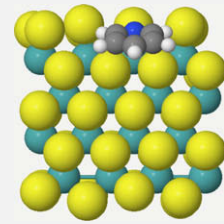
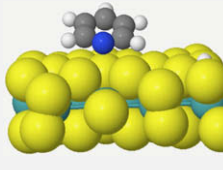
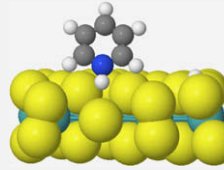
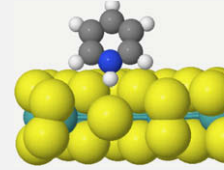
**Table 2**

The most stable adsorption sites and energies of pyridinium ( $C_5H_5N-H^+$ ) adsorbed on the Mo-edge terminated by sulfur dimers. The effect of adsorbed hydrogen close to the pyridinium is also shown.

Configuration	a	b	c	d	
Mo-edge with S-dimers					
Top view					
Side view	H coverage (%) $\Delta E_{ads}$ (eV)	12.5 -1.23	12.5 -1.10	0 -0.70	0 -0.65

**Table 3**

Adsorption sites and energies of pyridine (a) and pyridinium (b and c) on a Mo-edge containing S-dimers with one sulfur vacancy. Other less stable configurations are given in the Supplementary material.

Configuration	a: Pyridine	b: Pyridinium	c: Pyridinium	
Mo-edge with S-dimers and a sulfur vacancy				
Top view				
Side view	H coverage (%) $\Delta E_{ads}$ (eV)	14.3 -0.03	14.3 -1.51	0 -1.17

stronger on the fully saturated Mo-edge with the sulfur dimers than pyridine itself. We assume that the formation of pyridinium from adsorbed hydrogen and pyridine has a low activation energy in accordance with the results presented in Ref. [51].

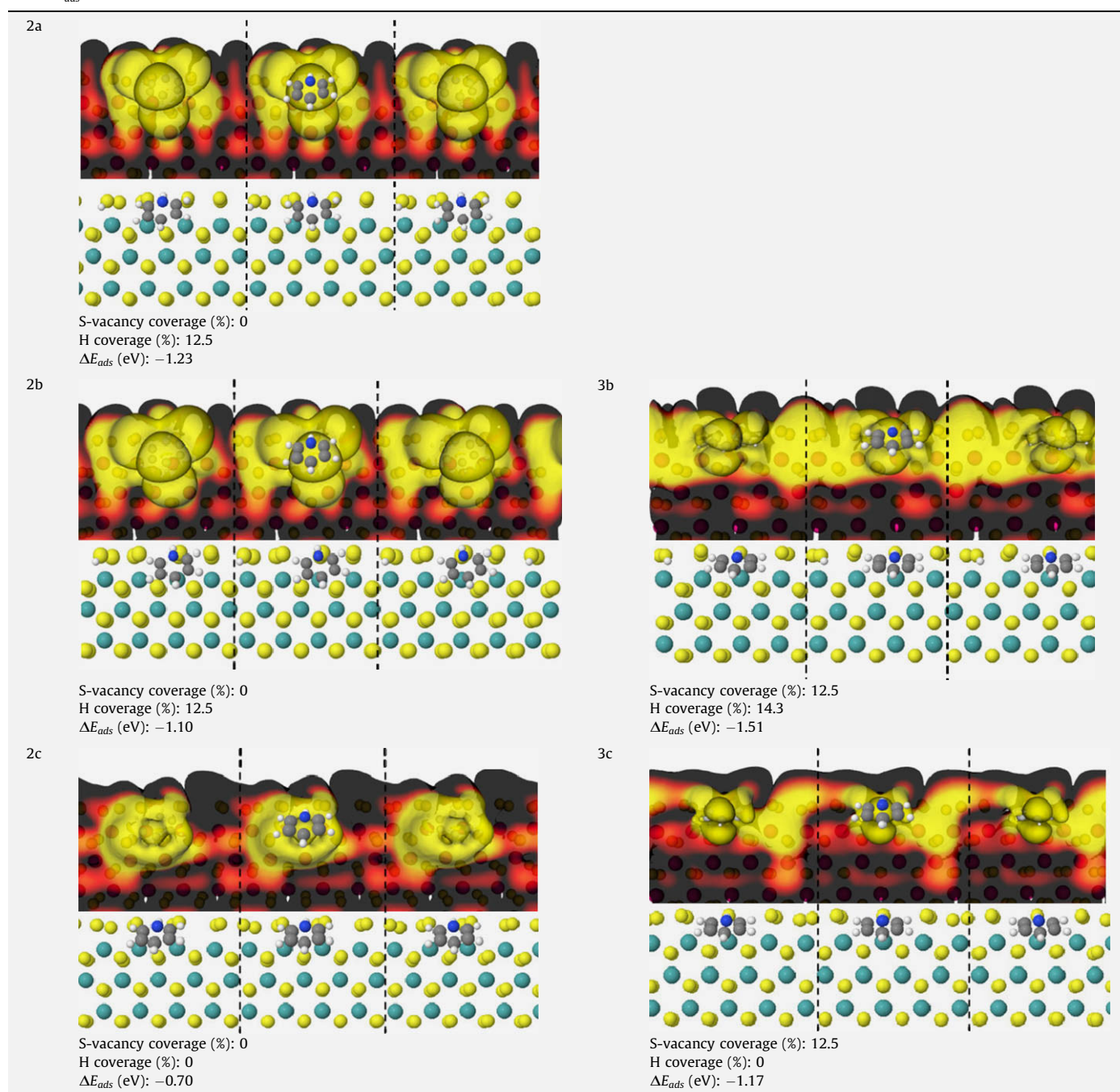
DFT calculations for pyridine and pyridinium adsorption on a sulfur vacancy on the Mo-edge are presented in Table 3, and they show that pyridine does not bind to the vacancy sites. Interestingly, we find that the binding energy would be 0.5 eV more endothermic if we remove the adsorbed hydrogen atom located on the edge (configuration a in Table 3, see Supplementary material for further details). In contrast, pyridinium binds strongly to sulfur vacancies, as shown in configurations b and c in Table 3. Thus, independent of whether the adsorption takes place on S–H groups on the fully saturated Mo-edge with the sulfur dimers or whether it occurs on the sulfur vacancies, pyridinium always binds much more strongly to the brim edge structures than pyridine.

From a detailed comparison of the features observed in the STM images in Fig. 3c and those in the STM simulations in Table 4, we conclude that only configuration 2a seems to be compatible with

the experimentally recorded STM images. In this configuration, the maximum of the bright protrusion associated with the pyridinium ion is indeed located at the position between the edge and brim state and in a lateral position between the S-dimers (see close-ups of the experimental STM image in Fig. 3c). We note that STM simulations of the static structure of a molecule predicted from the DFT results often produce a detailed intra-molecular contrast that is generally not observed in the experimental STM images recorded at 200 K where thermal vibrations are still quite substantial, which may explain the deviations between the experimental and detailed theoretical STM contours. Although adsorption of pyridinium in a S-vacancy is also favored thermodynamically in configuration 3b, the simulation of this configuration is clearly not compatible with the experimental STM contour, since the simulated STM image of the molecule reflects a structure that is located too close to the edge. We therefore attribute the species observed in the STM experiment to pyridinium adsorbed on top of the MoS<sub>2</sub> nanocluster to configuration 2a in Table 4. The atomic-scale insight gained from the present model



**Table 4**  
 Simulated STM images of pyridinium on the Mo-edge with S-dimers with relative adsorption energies and %H coverages using a  $4 \times 6$  unit cell that is shown by black dashed lines.  $\Delta E_{ads}$  is calculated for the  $4 \times 4$  unit cell.



studies thus shows that pyridine alone does not interact strongly with MoS<sub>2</sub> nanocluster edges, whereas pyridinium ions adsorb strongly on the brim sites of the MoS<sub>2</sub> nanoclusters. This explains why pyridine may act as a severe inhibitor for HYD reactions of sulfur-bearing molecules that preferentially take place on such brim sites.

### 3.1.3. Comparison of DFT calculations with IR observations on pyridine adsorption and pyridinium formation

To extend these model studies further and to investigate whether the presence of pyridinium is prevalent also at real HDS process conditions, we have carried out a theoretical analysis of IR-data for pyridine adsorbed on MoS<sub>2</sub> nanoclusters under hydroge-

nating conditions with a hydrogen/sulfur ratio similar to typical HDS conditions. The detailed edge structure and the shape of the MoS<sub>2</sub> nanoclusters have previously been shown to depend critically on the reaction conditions [49], which may influence the adsorption properties of pyridine and pyridinium compared to the studies on the model systems in the previous section. According to previous experimental findings [49] and calculated phase diagrams [44,50], MoS<sub>2</sub> nanoclusters adopt a hexagonal shape exposing both low-index edges, the (10 $\bar{1}$ 0) Mo-edge termination and the ( $\bar{1}$ 010) S-edge termination under typical industrial HDS conditions [44,50]. The S-edge is found to be saturated with S-dimers (with 100% H coverage), whereas the Mo-edge is terminated with S-monomers (with a partial H coverage as discussed in Refs. [49,44,65]).

Logadottir et al. [51] previously showed that adsorption of pyridine and formation of pyridinium were much more favorable on the Mo-edge than on the S-edge. The S-H groups on the S-edge do not react with pyridine since hydrogen is too strongly bound to sulfur on this edge termination of MoS<sub>2</sub> making hydrogen transfer less favorable, and therefore, we do not expect pyridine to be present on the S-edge under any conditions. The absence of a strong interaction between pyridine and the S-edge is confirmed in STM experiments when exposing the hexagonal MoS<sub>2</sub> nanoclusters formed under hydrogenating conditions [49] to pyridine (not shown). On the other hand, the studies by Logadottir et al. [51] clearly show a preference for pyridinium to interact with partially sulfided Mo-edge covered with S-monomers. The energy barrier of pyridinium formation is very small (less than 0.1 eV), and thus, pyridinium can easily form. Here, we elaborate on these results by recalculating the relevant structures for adsorption of pyridine and pyridinium on the Mo-edge with tighter force convergence parameters (which was computationally very expensive several years ago but which now can be readily be performed). These more elaborate DFT calculations allow us to calculate accurate vibrational frequencies for the pyridine and pyridinium molecules.

Previous IR-spectroscopy results [34] have shown evidence for the presence of pyridinium on the Mo-edge. In Fig. 4, the IR spectrum of pyridine adsorbed at 423 K on the sulfided Mo/Al<sub>2</sub>O<sub>3</sub> catalyst is compared to the calculated frequencies for pyridine and pyridinium. The equilibrium structures, adsorption energies and calculated vibrational frequencies used in the comparison are listed in Table 5. For the improved equilibrium structures, we find that they are very similar to those found in Ref. [51]. Also, the adsorption energies are found to be very similar and only change slightly due to improved computational accuracy. Regarding the calculated vibrational frequencies, we list the frequencies in the range of interest 1400–1650 cm<sup>-1</sup> for comparison with experimentally recorded IR results in Table 5.

We assign the calculated frequencies to the experimentally observed peaks as follows:

- The experimental frequency of 1546 cm<sup>-1</sup> is specific to pyridinium, and it is calculated to be 1534 cm<sup>-1</sup> by DFT. Pyridine adsorbed on MoS<sub>2</sub> does not exhibit any frequencies in this range.
- The experimental frequency of 1449 cm<sup>-1</sup> is matched very well by the calculated frequency of 1435 cm<sup>-1</sup>, which corresponds to adsorbed pyridine. Adsorbed pyridinium on MoS<sub>2</sub> does not exhibit any frequencies in this range.
- The experimental peaks at 1494 and 1621 cm<sup>-1</sup> may be constituted by several overlapping peaks. We assign these to the calculated frequencies 1467, 1591 cm<sup>-1</sup> for pyridine and 1474, 1616 cm<sup>-1</sup> for pyridinium. These two peaks are thus constituted by both pyridine and pyridinium and can therefore not be used to distinguish between the two.

The IR band at 1546 cm<sup>-1</sup> thus clearly shows the presence of pyridinium ions. From previous IR adsorption studies of pyridine on the alumina support surfaces only [66,67] and the IR study on MoS<sub>2</sub>/Al<sub>2</sub>O<sub>3</sub> [18,34], it is known that the 1546-cm<sup>-1</sup> pyridinium band only appears in the presence of MoS<sub>2</sub>. Thus, our results provide strong evidence for the presence of pyridinium adsorbing onto a Brønsted acid site on the MoS<sub>2</sub> catalyst. Based on these findings, the immediate conclusion would be that pyridine and pyridinium coexist on MoS<sub>2</sub>. However, if one compares IR studies with pyridine adsorption on the alumina support only [18,34,66,67] with the IR results of pyridine on MoS<sub>2</sub>/Al<sub>2</sub>O<sub>3</sub>, it is revealed that pyridinium peaks are only observed on MoS<sub>2</sub>/Al<sub>2</sub>O<sub>3</sub> and not on alumina, whereas the pyridine-related peaks are present in both cases.

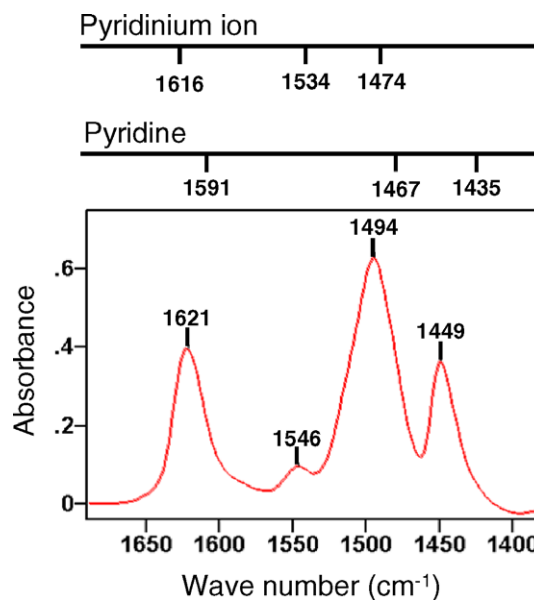


Fig. 4. IR spectrum of pyridine adsorption on MoS<sub>2</sub>/Al<sub>2</sub>O<sub>3</sub> adapted from Ref. [34]. The DFT calculated frequencies for adsorbed pyridine and pyridinium are included in the above bar diagram.

### 3.2. Electron density analysis of pyridinium bonding

The adsorption modes of pyridine and other N-cyclic compounds have previously been found [16,51] to involve either perpendicular [68] or parallel [69] bonding configurations on Mo/Al<sub>2</sub>O<sub>3</sub> and MoO<sub>3</sub>/Al<sub>2</sub>O<sub>3</sub> systems. It is generally assumed that nitrogenous compounds adsorb perpendicularly to the surface site through the interaction of the lone electron pair on the nitrogen, which is succeeded by the C–N cleavage. Adsorption of pyridine on metals occurs through nitrogen lone electron pair. The flat adsorption of N-cyclic compounds is related to the hydrogenation pathway through the  $\pi$ -aromatic system followed by C–N scission in a perpendicular mode. Our DFT results show that the pyridinium ion binds in a tilted mode rather than just parallel or perpendicular on the brim sites. The Mo-edges with a sulfur vacancy have a more pronounced effect on the pyridinium binding. The top adsorption on a S-vacancy (Table 3, configuration b) is more perpendicular with an angle of 85°, while the top adsorption on a non-vacancy (Table 2, configuration b) has an angle of 115° between C<sub>5</sub>H<sub>5</sub>NH-S-Mo atoms (S and Mo belong to the planar lattice). The charge density difference plots, depicted in Fig. 5, display the enhanced electron transfer to the catalyst when pyridinium is adsorbed on a sulfur vacancy, which is consistent with stronger binding energy on this site.

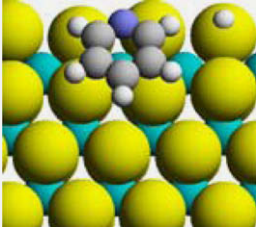
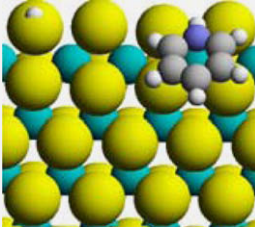
The interaction of pyridine and heavier basic N-containing molecules with NiMoS was studied recently in Refs. [25,70], and pyridine was found to adsorb perpendicular to the basal plane on a Ni atom through its nitrogen, whereas quinoline, indole and acridine mostly adsorb in a flatter or tilted configuration. Basic compounds were found to adsorb through their nitrogen, which is also true in our case. The strong interaction between the nitrogen and nickel allows faster hydrogenation of N-rings in these compounds than that of the phenyl-rings [70], and the hydrogen supplied by adsorbed H<sub>2</sub>S results in the lowest activation barrier.

### 3.3. Implications for HDS reaction pathways and inhibition

In all cases studied, both with and without a sulfur vacancy, pyridine adsorption was found to be endothermic, thermo-neutral



**Table 5**  
The relative adsorption energies and the vibrational frequencies of pyridine and pyridinium adsorbed on Mo-edge S-monomers calculated by DFT are shown. Adsorption energies are referenced to the clean MoS<sub>2</sub> edge and pyridine/pyridinium in the gas phase.

	a: Pyridine	b: Pyridinium
Mo-edge with S-monomers		
Top views with 25% H coverage		
$\Delta E_{ads}$ (eV)	-0.13	-0.59
IR frequencies (calculated, cm <sup>-1</sup> )	1435, 1467, 1591	1474, 1534, 1616

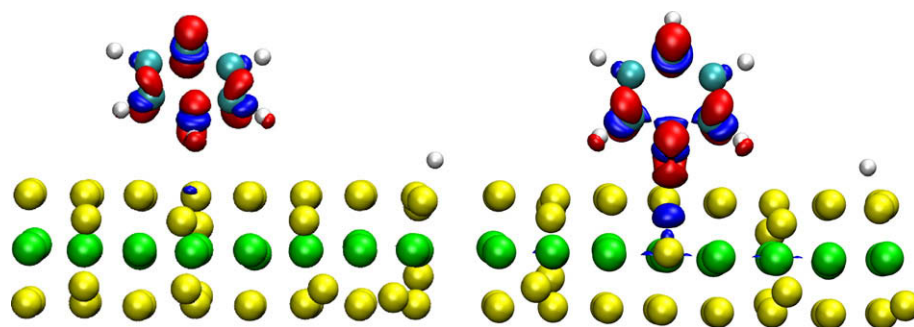


**Fig. 5.** Pyridinium electron density difference plot. Left: Pyridinium on Mo-edge with S-dimers (see Table 3, configuration b). Right: Pyridinium on Mo-edge with S-dimers on a S-vacancy (see Table 4, configuration b). Color code: Depletion of electron density (red) plotted at a contour value of  $-0.03 \text{ e}^3/\text{\AA}$ , increase in electron density (blue) plotted at a contour value of  $0.03 \text{ e}^3/\text{\AA}$ . (For interpretation of the references to color in this figure legend, the reader is referred to the web version of this article.)

or slightly exothermic, whereas pyridinium adsorption always was strongly exothermic. Under HDS conditions, pyridine and possibly also other N-cyclic compounds will scavenge available protons while the created pyridinium ions appear to block brim edge sites, and to a lesser extent vacancy sites, thereby inhibiting either or both of the hydrogenation or direct desulfurization pathways. This explains why the hydrogenation activity of MoS<sub>2</sub> catalysts is severely inhibited with N-containing basic compounds such as pyridine or quinoline [26,71] as revealed in the literature. Protonated N-cyclic species consume the hydrogen atoms and block the active sites. The HYD pathway on the Mo-edge is greatly affected by the adsorption of these protonated nitrogenous species under all HDS conditions, since the formation and adsorption of pyridinium type inhibitors on the brim sites as well as on the vacancies, and the creation of vacancies, originate from the availability of surface hydrogen on this particular edge.

The increased atomic-scale insight into inhibition mechanism by pyridine has also implications for Type I/Type II catalysts [53]. DFT calculations have been used to gain insight into support interaction with alumina and other supports, either modeled by simple models for the Mo–O–Al linkages [53,72] or by considering full alumina and titania substrates [73–75], and it was shown that the Mo–O–Al linkages quench the brim states [53]. The interaction of MoS<sub>2</sub> nanoclusters with alumina support can be described as a competition between the formation of chemical linkages, preferably in an epitaxial spacing, and van der Waals interactions for flat-lying MoS<sub>2</sub> [73–75]. Joshi et al. demonstrated subsequently that the thiolysis energy is a good measure for the tendency of a support material to form chemical linkages [72]. Even though the detailed sulfide-support interactions are still being debated, there

seems to be agreement on that chemical linkages change the edge structure profoundly and may lower both reactivity and inhibition by nitrogenous molecules.

#### 4. Conclusions

The interplay of STM studies and DFT calculations has provided detailed atomic-scale insight into the interaction of pyridine with the catalytically active sites on MoS<sub>2</sub> nanoclusters. Atom-resolved STM results show that pyridine molecules only adsorb weakly on the MoS<sub>2</sub> edges. However, in the presence of SH groups on the edges, new chemisorbed species are observed on the brim sites. According to DFT calculations and simulated STM images and comparison of these to experimentally recorded STM images, these species are assigned to pyridinium ions adsorbed on the brim sites at the edges of the MoS<sub>2</sub> nanoclusters. Thus, the present STM and DFT results have provided the first direct observation of pyridinium ions and thereby support the earlier IR and DFT findings that pyridinium ions are indeed formed on the Mo-edge of the MoS<sub>2</sub> nanoclusters. We find that the most favorable binding mode for pyridinium is in a tilted fashion adsorbed on top of the MoS<sub>2</sub> nanoclusters on the brim sites. Furthermore, excellent agreement is obtained between the calculated vibrational frequencies for pyridine and pyridinium and those observed in previous IR studies on high surface area MoS<sub>2</sub>/Al<sub>2</sub>O<sub>3</sub> catalysts. The finding that the IR peak at  $1546 \text{ cm}^{-1}$  can only be assigned to pyridinium further reveals that the main HDS inhibitor for the MoS<sub>2</sub> catalyst is pyridinium and not pyridine itself. The fact that the previous DFT calculations by Logadottir et al. [51] showed a very modest activation barrier

for pyridinium formation, in contrast to the experimental IR results, could be related to support effects that were not included in the DFT calculations.

Pyridinium adsorption on the Mo-brim edge sites has a twofold effect in the overall poisoning of the HDS catalyst: Firstly, the adsorption consumes atomically adsorbed hydrogen, which potentially could be used in hydrogenation, and secondly, the adsorbed pyridinium species block the hydrogenation pathway sites by binding strongly to the MoS<sub>2</sub> brim sites. In view of the present results, heavier cyclic nitrogenous compounds are suggested to be even stronger poisons than pyridine, because they have more delocalized  $\pi$ -character, which promotes the van der Waals interaction with the MoS<sub>2</sub> nanoclusters, and as a result, they bind more strongly to the catalytically active brim sites [15,16]. These compounds have also increasing proton affinity, making them stronger inhibitors for the hydrogenation pathway. We are currently extending these studies to include heavier N-cyclic compounds and Co- or Ni-promoted MoS<sub>2</sub> nanoclusters.

### Acknowledgments

The iNANO group gratefully acknowledges financial support from The Danish Research Councils, The Strategic Research Council (NABIIT project “Development of new metal-oxide and -sulphide catalysts”), the Carlsberg Foundation, the Lundbeck Foundation and the Villum-Kahn Rasmussen Foundation. JVL and FB both acknowledge generous financial support from the European Research Council (ERC).

### Appendix A. Supplementary material

Supplementary data associated with this article can be found, in the online version, at doi:10.1016/j.jcat.2010.02.007.

### References

- [1] H. Topsøe, B.S. Clausen, F.E. Massoth, *Hydrotreating Catalysis*, Springer Verlag, Berlin, 1996.
- [2] R. Carr, *IVT Int.* 11 (2008) 22. <[http://www.euromot.org/download/news/furtherpub/IVT08-11\\_EU\\_Fuel\\_Quality\\_Directive.pdf](http://www.euromot.org/download/news/furtherpub/IVT08-11_EU_Fuel_Quality_Directive.pdf)>.
- [3] M.V. Landau, *Catal. Today* 36 (1997) 393.
- [4] B.C. Gates, H. Topsøe, *Polyhedron* 16 (1997) 3213.
- [5] D.D. Whitehurst, T. Isoda, I. Mochida, *Adv. Catal.* 42 (1998) 345.
- [6] T. Kabe, A. Ishihara, W. Qian, *Hydrodesulfurization and Hydrogenation*, Wiley-CH, Kodanska, 1999.
- [7] K.G. Knudsen, B.H. Cooper, H. Topsøe, *Appl. Catal. A* 189 (1999) 205.
- [8] S.F. Venner, *Hydrocarb. Process.* 79 (2000) 51.
- [9] I.V. Babich, J.A. Moulijn, *Fuel* 82 (2003) 607.
- [10] C. Song, *Catal. Today* 86 (2003) 211.
- [11] R.G. Leliveld, S.E. Eijssbouts, *Catal. Today* 130 (2008) 183.
- [12] M. Houalla, N.K. Nag, A.V. Sapre, D.H. Broderick, B.C. Gates, *AIChE J.* 24 (1978) 1015.
- [13] M. Houalla, D.H. Broderick, A.V. Sapre, N.K. Nag, V.H.J. de Beer, B.C. Gates, H. Kwart, *J. Catal.* 61 (1980) 523.
- [14] X. Ma, K. Sakanishi, I. Mochida, *Indus. Eng. Chem. Res.* 35 (1996) 2487.
- [15] M. Nagai, T. Kabe, *J. Catal.* 81 (1983) 440.
- [16] V. La Vopa, C.N. Satterfield, *J. Catal.* 110 (1988) 375.
- [17] T. Kabe, A. Ishihara, H. Tajima, *Ind. Eng. Chem. Res.* 31 (1992) 1577.
- [18] N.Y. Topsøe, H. Topsøe, *J. Catal.* 139 (1993) 641.
- [19] V. Meille, E. Schulz, M. Lemaire, M. Vrinat, *J. Catal.* 170 (1997) 29.
- [20] F. Van Looij, P. Van Der Laan, W.H.J. Stork, D.J. DiCamillo, J. Swain, *Appl. Catal. A: General* 170 (1998) 1.
- [21] H. Schulz, W. Böhringer, P. Waller, F. Ousmanov, *Catal. Today* 49 (1999) 87.
- [22] P. Zeuthen, K.G. Knudsen, D.D. Whitehurst, *Catal. Today* 65 (2001) 307.
- [23] M. Egorova, R. Prins, *J. Catal.* 225 (2004) 417.
- [24] T.C. Ho, *Catal. Today* 98 (2004) 3.
- [25] M. Sun, A.E. Nelson, J. Adjaye, *Catal. Lett.* 109 (2006) 133.
- [26] M. Nagai, T. Sato, A. Aiba, *J. Catal.* 97 (1986) 52.
- [27] G. Perot, *Catal. Today* 10 (1991) 447.
- [28] A. Amorelli, Y.D. Amos, C.P. Halsig, J.J. Kosman, R.R.J. Jonke, M. DeWind, J. Vrieling, *Hydrocarb. Process.* 71 (1992) 93.
- [29] I. Mochida, K. Sakanishi, X. Ma, S. Nagao, T. Isoda, *Catal. Today* 29 (1996) 185.
- [30] P. Wiwel, K. Knudsen, P. Zeuthen, D. Whitehurst, *Indus. Eng. Chem. Res.* 39 (2000) 533.
- [31] R. Prins, *Adv. Catal.* 46 (2001) 399.
- [32] M. Breyse, G. Djega-Mariadassou, S. Pessayre, C. Geantet, M. Vrinat, G. Perot, M. Lemaire, *Catal. Today* 84 (2003) 129.
- [33] B.H. Cooper, K.G. Knudsen, in: C.S. Hsu, P.R. Robinson (Eds.), *Practical Advances in Petroleum Processing*, Springer, New York, 2006, p. 866.
- [34] N.Y. Topsøe, H. Topsøe, F.E. Massoth, *J. Catal.* 119 (1989) 252.
- [35] G. Berhault, M. Lacroix, M. Breyse, F. Mauge, J.C. Lavalley, H. Nie, L. Qu, *J. Catal.* 178 (1998) 555.
- [36] X.L. Ma, H.H. Shobert, *ACS Div. Petrol. Chem. Prepr.* 213 (1997) 15.
- [37] S. Helveg, J.V. Lauritsen, E. Lægsgaard, I. Stensgaard, J.K. Nørskov, B.S. Clausen, H. Topsøe, F. Besenbacher, *Phys. Rev. Lett.* 84 (2000) 951.
- [38] J.V. Lauritsen, M. Nyberg, R.T. Vang, M.V. Bollinger, B.S. Clausen, H. Topsøe, K.W. Jacobsen, E. Lægsgaard, J.K. Nørskov, *Nanotechnology* 14 (2003) 385.
- [39] J.V. Lauritsen, M. Nyberg, J.K. Nørskov, B.S. Clausen, H. Topsøe, E. Lægsgaard, F. Besenbacher, *J. Catal.* 224 (2004) 94.
- [40] J.V. Lauritsen, F. Besenbacher, *Adv. Catal.* 50 (2006) 97.
- [41] L.S. Byskov, B. Hammer, J.K. Nørskov, B.S. Clausen, H. Topsøe, *Catal. Lett.* 47 (1997) 177.
- [42] L.S. Byskov, J.K. Nørskov, B.S. Clausen, H. Topsøe, *J. Catal.* 187 (1999) 109.
- [43] M.V. Bollinger, J.V. Lauritsen, K.W. Jacobsen, J.K. Nørskov, S. Helveg, F. Besenbacher, *Phys. Rev. Lett.* 87 (2001) 196803.
- [44] M.V. Bollinger, K.W. Jacobsen, J.K. Nørskov, *Phys. Rev. B* 67 (2003) 854101.
- [45] P. Raybaud, J. Hafner, G. Kresse, S. Kasztelan, H. Toulhoat, *J. Catal.* 189 (2000) 129.
- [46] M. Sun, J. Adjaye, A.E. Nelson, *Appl. Catal. A: General* 263 (2004) 131.
- [47] M. Sun, A.E. Nelson, J. Adjaye, *Catal. Today* 105 (2005) 36.
- [48] B. Hinnemann, P.G. Moses, J.K. Nørskov, *J. Phys.: Condens. Matter* 20 (2008) 064236.
- [49] J.V. Lauritsen, M.V. Bollinger, E. Lægsgaard, K.W. Jacobsen, J.K. Nørskov, B.S. Clausen, H. Topsøe, F. Besenbacher, *J. Catal.* 221 (2004) 510.
- [50] P.G. Moses, B. Hinnemann, H. Topsøe, J.K. Nørskov, *J. Catal.* 248 (2007) 188.
- [51] Á. Logadóttir, P.G. Moses, B. Hinnemann, N.Y. Topsøe, K.G. Knudsen, H. Topsøe, J.K. Nørskov, *Catal. Today* 111 (2006) 44.
- [52] E. Lægsgaard, F. Besenbacher, K. Mortensen, I. Stensgaard, *J. Microsc.* 152 (1988) Pt 3.
- [53] B. Hinnemann, J.K. Nørskov, H. Topsøe, *J. Phys. Chem. B* 109 (2005) 2245.
- [54] B. Hammer, L.B. Hansen, J.K. Nørskov, *Phys. Rev. B* 59 (1999) 7413.
- [55] S.R. Bahn, K.W. Jacobsen, *Comput. Sci. Eng.* 4 (2002) 56.
- [56] H.J. Monkhorst, J.D. Pack, *Phys. Rev. B* 13 (1976) 5188.
- [57] D. Vanderbilt, *Phys. Rev. B* 41 (1990) 7892.
- [58] N. Troullier, J.L. Martins, *Phys. Rev. B* 43 (1991) 1993.
- [59] J.P. Perdew, J.A. Chevary, S.H. Vosko, K.A. Jackson, M.R. Pederson, D.J. Singh, C. Fiolhais, *Phys. Rev. B* 46 (1992) 6671.
- [60] J. Tersoff, D.R. Hamann, *Phys. Rev. Lett.* 50 (1983) 1998.
- [61] J. Tersoff, D.R. Hamann, *Phys. Rev. B* 31 (1985) 805.
- [62] F. Besenbacher, M. Brorson, B.S. Clausen, S. Helveg, B. Hinnemann, J. Kibsgaard, J.V. Lauritsen, P.G. Moses, J.K. Nørskov, H. Topsøe, *Catal. Today* 130 (2008) 86.
- [63] W. Humphrey, A. Dalke, K. Schulten, *J. Mol. Graphics* 14 (1996) 33.
- [64] E. Willighagen, M. Howard, *Jmol: an open-source Java viewer for chemical structures in 3D*, <<http://www.jmol.org/>>.
- [65] B. Hinnemann, P.G. Moses, J. Bonde, K.P. Jørgensen, J.H. Nielsen, S. Hørch, I. Chorkendorff, J.K. Nørskov, *J. Am. Chem. Soc.* 127 (2005) 5308.
- [66] E.P. Parry, *J. Catal.* 2 (1963) 371.
- [67] E. Kassab, M. Castellà-Ventura, *J. Phys. Chem. B* 109 (2005) 13716.
- [68] T. Fransen, O. Van Der Meer, P. Mars, *J. Phys. Chem.* 80 (1976) 2103.
- [69] M.J. Ledoux, P.E. Puges, G. Maire, *J. Catal.* 76 (1982) 285.
- [70] M. Sun, A.E. Nelson, J. Adjaye, *Catal. Today* 109 (2005) 49.
- [71] M.J. Girgis, B.C. Gates, *Ind. Eng. Chem. Res.* 30 (1991) 2021.
- [72] Y.V. Joshi, P. Ghosh, M. Daage, W.N. Delgass, *J. Catal.* 257 (2008) 71.
- [73] C. Arrouvel, M. Digne, M. Breyse, H. Toulhoat, P. Raybaud, *J. Catal.* 222 (2004) 152.
- [74] C. Arrouvel, M. Breyse, H. Toulhoat, P. Raybaud, *J. Catal.* 232 (2005) 161.
- [75] D. Costa, C. Arrouvel, M. Breyse, H. Toulhoat, P. Raybaud, *J. Catal.* 246 (2007) 325.